HHS Public Access

Author manuscript

Eur J Clin Invest. Author manuscript; available in PMC 2016 March 29.

Published in final edited form as:

Eur J Clin Invest. 2008 April ; 38(4): 211–217. doi:10.1111/j.1365-2362.2008.01930.x.

Ovariectomy increases vascular calcification via the OPG/RANKL cytokine signalling pathway

B. G. Choi, **G. Vilahur**[*], **L. Cardoso**, **J. C. Fritton**, **B. Ibanez**, **M. U. Zafar**, **D. Yadegar**, **W. S. Speidl**, **M. B. Schaffler**, **V. Fuster**, and **J. J. Badimon**

Mount Sinai School of Medicine, New York, USA

[*]Hospital de la Santa Creu i Sant Pau, Barcelona, Spain

Abstract

Background—Observational studies suggest a strong relationship between menopause and vascular calcification. Receptor activator of nuclear factor-κB ligand (RANKL) and osteoprotegerin (OPG) are critical regulators of bone remodelling and modulate vascular calcification. We assessed the hypothesis that ovariectomy increases vascular calcification via the OPG/RANKL axis.

Materials and methods—Age-matched sexually mature rabbits were randomized to ovariectomy (OVX, $n = 12$) or sham procedure (SHAM, $n = 12$). One month post-procedure, atherosclerosis was induced by 15 months 0·2%-cholesterol diet and endothelial balloon denudations (at months 1 and 3). Aortic atherosclerosis was assessed *in vivo* by magnetic resonance imaging (MRI) at months 9 and 15. At sacrifice, aortas were harvested for *ex vivo* microcomputed tomography (μCT) and molecular analysis of the vascular tissue.

Results—Vascular calcification density and calcific particle number were significantly greater in OVX than SHAM (8·4 ± 2·8 vs. 1·9 ± 0·6 mg cm^{-3}, $P = 0·042$, and 94 ± 26 vs. 33 ± 7 particles cm^{-3}, $P = 0·046$, respectively). Calcification morphology, as assessed by the arc angle subtended by the largest calcific particle, showed no difference between groups (OVX 33 ± 7° vs. SHAM 33 ± 5°, $P = 0·99$). By Western blot analysis, OVX increased the vascular OPG:RANKL ratio by 66%, $P = 0·029$, primarily by decreasing RANKL ($P = 0·019$). At month 9, MRI demonstrated no difference in atheroma volume between OVX and SHAM, and no significant change was seen by the end of the study.

Conclusions—In contrast to bone, vascular OPG:RANKL ratio increased in response to ovariectomy with a corresponding fourfold increase in arterial calcification. This diametrical organ-specific response may explain the comorbid association of osteoporosis with calcifying atherosclerosis in post-menopausal women.

Correspondence to: Juan J. Badimon, PhD, One Gustave L. Levy Place, Box 1030, New York, NY 10029. Tel.: (212) 241-8484 Voice; fax: (212) 426-6962; juan.badimon@mssm.edu.

Address

Cardiovascular Biology Research Laboratory (B. G. Choi, B. Ibanez, M. U. Zafar, D. Yadegar, W. S. Speidl, J. J. Badimon); Zena and Michael A. Wiener Cardiovascular Institute (B. G. Choi, M. U. Zafar, V. Fuster, J. J. Badimon); Leni and Peter W. May Department of Orthopaedics, Mount Sinai School of Medicine, New York, NY (L. Cardoso, J. C. Fritton, M. B. Schaffler).

Keywords

Atherosclerosis; menopause; osteoporosis; vascular calcification

Introduction

Elevated coronary calcium score, as assessed by computed tomography, has been associated with an increased risk of cardiovascular events [1]. Menopause has also been associated with increased cardiovascular risk with one in two post-menopausal women having cardiovascular disease [2], and loss of endogenous ovarian production of sex hormones has been correlated with increased coronary calcification [3]. Menopause is also a well established risk factor for osteoporosis [4], leading to the curiously concomitant phenomenon of skeletal orthotopic bone loss and vascular heterotopic bone formation. As macrophages in atherosclerotic lesions undergo osteoclastic differentiation [5], a possibility is raised that cytokine signalling pathways that regulate orthotopic bone remodelling may also influence vascular calcification formation. The receptor activator of nuclear factor-κB ligand (RANKL) is an essential cytokine in osteoclastogenesis and subsequent bone resorption, and its soluble decoy osteoprotegerin (OPG) prevents bone loss, making the ratio of OPG:RANKL instrumental in the assessment of osteoclast activity and its role in osteoporosis [6].

Since decreased RANKL is associated with increased coronary artery disease [7] and increased OPG is also associated with increased coronary artery disease (CAD) severity [8], we examined in this experiment whether the OPG/RANKL cytokine signalling pathway influences atherosclerotic vascular calcification in a model of post-menopausal osteoporosis and experimental atherosclerosis.

Materials and methods

Study design

After reaching sexual maturity (age 5 months, 3·3 ± 0·2 kg), female New Zealand White rabbits (Covance Research Products, Denver, PA, USA) were randomized to ovariectomy (OVX, $n = 12$) or sham procedure (SHAM, $n = 12$). One month post-operatively, aortic atherosclerotic lesions were induced by 0·2% cholesterol-enriched rabbit diet (WIL Research Laboratories, Ashland, OH, USA) and double balloon-induced aortic endothelial denudation as previously described [9–14]. All procedures were performed under general anaesthesia by intramuscular injection of acepromazine (1 mg kg^{-1}; Boehringer Ingelheim Vetmedica, St. Joseph, MO, USA); ketamine (20 mg kg^{-1}; Fort Dodge Animal Health, Fort Dodge, IA, USA), and xylazine (2 mg kg^{-1}; Lloyd Laboratories, Shenandoah, IA, USA). This experimental model of atherosclerosis has reliably demonstrated reproducible development of advanced atherosclerotic lesions [9–14]. After nine months of atherosclerosis induction, initial assessment of atherosclerosis development was performed by magnetic resonance imaging (MRI) analysis. Six months later, all rabbits underwent repeat MRI analysis and were then sacrificed for histopathology, molecular study and *ex vivo* microcomputed tomography (μCT). Development of osteoporosis was confirmed by

μCT. Observers for all measurements (MRI, histopathology, Western blot and μCT) were blinded to the treatment group.

Magnetic resonance imaging

The animals were anaesthetized as above and placed supine in a 1·5-tesla MRI system (Siemens Medical Solutions, Malvern, PA, USA) using a conventional extremity coil. Gradient-echo coronal and sagittal images were used to localize the abdominal aorta, and sequential transverse images (3 mm thick) of the aorta were obtained from the celiac trunk to the iliac bifurcation using a fast spin-echo sequence (total imaging time 1 h) with an in-plane resolution of 230 × 230 μm [proton density weighted (PDW): TR/TE, 2300/5·6 ms; T1W: TR/TE, 800/5·6 ms; T2W: TR/TE, 2300/62 ms; field of view 12 × 12 cm; matrix 512 × 512; echo train length = 8; signal averages = 4]. T1W sequence was repeated 5 min after injection of gadopentetate dimeglumine (0·1 mmol kg^{-1}; Berlex Laboratories, Montville, NJ, USA). Fat suppression and flow saturation pulses were used as previously reported [10].

The MRIs were transferred to a Macintosh computer system (Apple, Cupertino, CA, USA) for analysis. The initial and final images were matched for anatomic position by using distances from the renal arteries and iliac bifurcation as previously validated [10], so that true serial data on atherosclerotic progression/regression could be obtained. The 6 cm of aorta immediately distal to the left renal artery, corresponding to 20 contiguous MRI segments, were selected for vessel wall measurements. Cross-sectional areas of the lumen and vessel wall were determined by a validated semiautomatic quantification method programmed on ImageJ (National Institutes of Health, Bethesda, MD, USA) that determined the lumen area and vessel wall area (vessel wall area = total vessel area – lumen area); the intra-observer variability for vessel wall measurement using this automated program was 2·1%, indicating high reproducibility of measurement [15]. For each animal at each time point, measurements from the 20 contiguous MRIs were averaged, and the mean values for each rabbit were considered for statistical analysis.

Micro-computed tomography

Within 24 h of the final MRI, the rabbits were euthanized by intravenous injection of 150 mg kg^{-1} sodium pentobarbital (Sleepaway, Fort Dodge Animal Health). Prior to euthanasia, the animals received heparin (100 U kg^{-1}; American Pharmaceutical Partners, Schaumberg, IL, USA) to prevent post-mortem thrombosis. The aortas were cannulated at the level of the diaphragm and immediately flushed proximally and distally with 250 mL of 0·1 M phosphate-buffered saline (PBS), pH 7·4. The abdominal aorta was further flushed with 250 mL of cold (4 °C) perfusion fixative at 100 mmHg (4% paraformaldehyde in PBS). Using anatomic landmarks observed by MRI, the abdominal aorta was excised, immersed in fresh fixative with preserved *in situ* configuration, and then stored at 4 °C for one week to fix the tissue. A 6 cm section distal to the left renal artery, which corresponded to the segment analysed by MRI, was then washed free of formaldehyde using distilled water and immersed in PBS prior to μCT image acquisition. X-ray images of the aorta were obtained using a GE Healthcare eXplore SP Pre-Clinical Specimen Micro-CT system (General Electric, London, ON, Canada). For image acquisition, 360 consecutive X-ray projections were obtained using an exposure time of 1·7 s, at 80 kVp and 80 mA, and a voxel resolution of 21 μm. For each

projection, five exposures were obtained and averaged to produce a high contrast low noise image. The raw images were corrected for possible pixel defects in the digital detector using bright and dark fields, and a standard reconstruction algorithm included in the GE analysis system was applied to generate three-dimensional volumes from the planar projections. Mineral density within the volumes was calibrated using a phantom containing hydroxyapatite, air and water, which was included with each scan. For the analysis of calcified tissue, the volume enclosing the entire 6 cm aorta segment was selected. Images were segmented into calcified and non-calcified tissue on each volume of interest using a global threshold method [16]. After calibration and identification of calcified tissue, the amount of calcium in the sample was quantified using the Tissue Mineral Content tool in the Advanced Bone Analysis software from GE Healthcare. Mineral organization in the volume was assessed using a method based upon a previously established analysis by intravascular ultrasound (IVUS) [17]. Three-dimensional images were reconstructed for the 20 contiguous 3 mm sections corresponding to the MRI slices; the largest arc of calcium in each cross-section was identified, and the arc was measured in degrees with a protractor centred on the vessel lumen.

Histopathology and immunohistochemistry

Following μCT, the aorta segment analysed by MRI and μCT was cut into 3 mm sections corresponding to the imaging analysis segments. Specimens were paraffin-embedded and cut into serial 5-μm thick sections. Within each 3 mm segment, a section was stained with Masson's trichrome elastic stain and additional sections stained immunohistochemically with RAM-11 antibody for macrophages (Dako, Carpenter, CA, USA), α-actin for vascular smooth muscle cells (Sigma-Aldrich, St Louis, MO, USA), and matrix metalloproteinase-1 (MMP-1, Laboratory Vision, Fremont, CA, USA). The abdominal aorta superior to the left renal artery was separately processed by Oil Red O method for lipid deposition. Histopathological analysis was performed using a computer-based quantitative colour image analysis system (ImageJ) to assess the percentage of stained area for each section.

Western blot analysis

Immediately after euthanasia, the descending thoracic aorta was flushed with physiological buffer as above and snap-frozen in liquid nitrogen. The frozen aortas were pulverized and homogenized in lysis buffer (50 mmol L^{-1} Tris-HCl, 1 mmol L^{-1} EDTA, 1% Triton X-100, 0·1 mg mL^{-1} PMSF, pH 7·4). Equal amounts of protein (50 μg $lane^{-1}$) estimated by bicinchoninic acid reagent (Pierce Biotechnology, Rockford, IL, USA) were loaded in 10% PAGE to quantify protein expression. Western blot analysis was performed with antibodies against bone morphogenetic protein-2 [BMP-2, Santa Cruz Biotechnology N-14 (sc-6895); Santa Cruz, CA, USA], cyclooxygenase-2 (COX-2, Transduction Laboratories #610203), monocyte chemoattractant protein-1 [MCP-1, Santa Cruz Biotechnology N-14 (sc-1785)], OPG [Santa Cruz Biotechnology N-20 (sc-8468)], and RANKL [Santa Cruz Biotechnology N-19 (sc-7628)]. After incubation with their respective peroxidase-labelled immunoglobulins, antibody visualization was performed by the chemiluminescent method SuperSignal® (Pierce Biotechnology) and evaluated by densitometry (ImageJ).

Statistical analysis

Measurements with multiple observations per rabbit (i.e. MRI, μCT, histopathology) were averaged so that each rabbit represented a single observation per time point. The paired *t*-test was used for the serial MRI measurements to compare within groups the change from initial imaging to study conclusion. After testing for normal distribution and equality of variances with Levene's *F*-test, the unpaired *t*-test was used for all single time point measurements (i.e. μCT, histopathology, Western blot) to compare between OVX and SHAM (SPSS v11·0·2; Chicago, IL, USA). All probabilities were two-sided with $P < 0{\cdot}05$ considered statistically significant. All values are expressed as mean ± standard error of the mean (SEM).

Ethical considerations

The study protocol was approved by the Institutional Animal Care and Use Committee of the Mount Sinai School of Medicine. The authors had full access to the data and take responsibility for its integrity. All authors have read and agree to the manuscript as written.

Results

Effects on plasma lipid levels, body weight and bone

There were no statistically significant differences in lipid parameters between OVX and SHAM (Table 1). There were no significant differences in body weight at baseline or end of follow-up. As expected, the OVX group experienced a decline in uterine weight and an increase in osteoporosis as described per similar ovariectomy models [18,19].

Changes in aorta vessel wall measured by serial MRI

No statistically significant differences in vessel wall dimensions were seen between OVX and SHAM (Table 2). Qualitative analysis of plaque composition by multicontrast MRI suggested increased lipid deposition (higher signal intensity in T1W and PDW and lower in T2W) in OVX compared to SHAM. Areas of vascular calcification (low signal intensity in T1W, T2W and PDW) were more pronounced in the OVX group. To confirm these differences in calcification, all aortas were examined by μCT.

Vascular calcification assessment by μCT

Mineralization was greatest in OVX, both by weight and particle number, compared to SHAM, but no differences in calcification morphology, as assessed by arc of calcium deposition, were observed (Table 3). In all groups, the areas of calcification predominated in the neointima. Representative μCT images are seen in Fig. 1.

Plaque composition

Confirming the observation by MRI, post-mortem histopathological analysis demonstrated an 80% increase ($P = 0{\cdot}008$) in lipid content (Oil Red O) and a 57% decrease ($P = 0{\cdot}0002$) in smooth muscle cell area (α-actin) in OVX compared to SHAM as seen in Fig. 2. No statistically different observations were made for macrophage content (RAM-11), but

macrophage activity as assessed by MMP-1 expression was increased in OVX by 130%, P = 0·010 (Fig. 2).

Plaque activity

A significant 66% increase in OPG:RANKL ratio was seen in OVX (P = 0·029), primarily driven by a decrease in RANKL by 36%, P = 0·019 (Fig. 3). When comparing OVX vs. SHAM, no differences were observed with other bone active proteins such as BMP-2 (0·37 ± 0·05 vs. 0·33 ± 0·06 arbitrary units, respectively), nor with measures of inflammation (i.e. COX-2: 0·47 ± 0·05 vs. 0·49 ± 0·02 and MCP-1: 0·40 ± 0·01 vs. 0·37 ± 0·02 arbitrary units, respectively).

Discussion

Consistent with epidemiological findings [3], our study demonstrates that loss of endogenous sex hormone production by experimental menopause (i.e. ovariectomy) results in increased aortic atherosclerotic calcification burden. The observed changes in OPG:RANKL vascular expression may explain this finding. Increased vascular calcification could possibly explain the increased incidence of cardiovascular events in women after menopause.

Increased mineralization within atherosclerotic lesions could potentially destabilize plaques leading to increased acute coronary syndrome (ACS). Microcalcifications, previously undetectable by prior methods but now visible by μCT, cause local stress concentrations that can dramatically lower the rupture threshold of vulnerable plaques [20]. The four-fold increase in vascular calcification seen in our model after ovariectomy may therefore represent a possible heightened risk of ACS consistent with the predictive accuracy of the coronary calcium score to determine risk of future cardiovascular events [1]. Recent prospective clinical trials, however, suggest that quantity of calcification alone may not completely explain this phenomenon.

In clinical trials which used the coronary calcium score as predetermined end points, intensive statin therapy which has been demonstrated to significantly reduce cardiovascular events [21,22], also significantly increased vascular calcification [23,24]. Thus, a paradox exists in which therapies known to reduce cardiovascular events (i.e. intensive statin therapy) also increase a marker for known cardiovascular risk (i.e. calcium score). A possible explanation for this paradox is that microcalcifications may increase the risk by decreasing the rupture threshold, but as calcifications coalesce, the rupture threshold increases since the surface area of the interface between calcification and other soft tissues decreases [5]. In our study, we found that the increase in calcification in the ovariectomized animals was driven primarily by particle number as opposed to particle size; therefore, unlike therapies which may increase calcification confluence [25], loss of endogenous sex hormone production may increase risk by increasing the quantity of plaque-destabilizing microcalcifications.

The increase in OPG:RANKL ratio as a possible explanation for the mechanism behind the increase in calcification in the ovariectomized group is intriguing on several levels. OPG

and RANKL are produced by vascular endothelial and smooth muscle cells, but the factors that lead to an inhibition of RANKL expression, which was the primary driver of the increased OPG/RANKL ratio with ovariectomy seen in our study, are unknown [26]. Inflammatory cytokines typically increase both vascular RANKL and OPG expression, but the inhibitory mechanisms to decrease RANKL expression remain an area of active investigation. Down-regulation of RANKL may prevent calcification resorption by osteoclast-like cells leading to increased mineral deposition. In bone, OPG:RANKL ratio is decreased after menopause resulting in osteoporosis [6], so our finding that the change in OPG:RANKL is opposite in vascular tissue may explain how osteoporosis and calcifying atherosclerosis can occur concurrently. Furthermore, treatments that target the OPG/RANKL cytokine signalling pathway for osteoporosis [27] may therefore yield unexpected and possibly unwanted effects upon vascular calcification.

Limitations

Although our study found an association between ovariectomy, change in OPG:RANKL and quantity of vascular calcification, causality has not been definitively determined. Such an experiment would require a RANKL inhibitor such as denosumab [27]; however, denosumab does not have activity against rabbit RANKL (Ralph Zitnik, MD, Amgen Inc., unpublished data, 2006). Nevertheless, the finding of increased calcification without change in calcification morphology is strongly consistent with increased OPG:RANKL and no change in BMP-2, as we have found in this experiment. Also, our analysis was performed on a per aorta basis and does not take into account that OPG and RANKL activity may be heterogeneous and higher in calcification border zones. Furthermore, as with all experimental animal models of human disease, a further limitation is that the model used did not have human cells and while suggestive of human atherosclerotic disease, is derived by experimental methods that do not replicate the time course and histopathological distribution of natural human atherosclerosis. However, this model is well validated [10–14], and similar experimentation in humans is unfeasible because of ethical considerations.

Conclusion

Our data show that ovariectomy results in increased vascular microcalcification, which may increase plaque vulnerability. This finding is consistent with epidemiological findings of increased vascular calcification after menopause and a subsequent rise in cardiovascular events. The possible mechanism behind this increased mineralization, an increase in the OPG:RANKL ratio, may have implications upon therapies that target this cytokine signalling pathway for treatment of bone disorders.

Acknowledgments

This study was made possible by NHLBI grant T32 HL007824 (to Dr Choi), and a contract within the Spanish Science and Education Ministry at the Institut Catala de Ciencies Cardiovasculars, Barcelona, Spain (to Dr Vilahur). Drs Choi and Vilahur contributed equally to this manuscript. The authors thank Jose Rodriguez, MD and Constantin Novoselsky, MD, for their help in the surgical procedures; Anthony Lopez for expert planimetry; Boris Cortes, MD for assistance with the molecular studies; and James Tunstead, PhD for immunohistochemistry. The authors would like to give special thanks to the staff of the Mount Sinai Center for Comparative Medicine & Surgery for dedicated animal care.

References

1. Redberg RF, Vogel RA, Criqui MH, Herrington DM, Lima JA, Roman MJ. 34th Bethesda Conference: Task force #3 – What is the spectrum of current and emerging techniques for the noninvasive measurement of atherosclerosis? J Am Coll Cardiol. 2003; 41:1886–98. [PubMed: 12798555]
2. Thom T, Haase N, Rosamond W, Howard VJ, Rumsfeld J, Manolio T, et al. Heart Disease and Stroke Statistics – 2006 Update. A Report from the American Heart Association Statistics Committee and Stroke Statistics Subcommittee. Circulation. 2006
3. Christian RC, Harrington S, Edwards WD, Oberg AL, Fitzpatrick LA. Oestrogen status correlates with the calcium content of coronary atherosclerotic plaques in women. J Clin Endocrinol Metab. 2002; 87:1062–7. [PubMed: 11889163]
4. Ahlborg HG, Johnell O, Turner CH, Rannevik G, Karlsson MK. Bone loss and bone size after menopause. N Engl J Med. 2003; 349:327–34. [PubMed: 12878739]
5. Abedin M, Tintut Y, Demer LL. Vascular calcification: mechanisms and clinical ramifications. Arterioscler Thromb Vasc Biol. 2004; 24:1161–70. [PubMed: 15155384]
6. Hofbauer LC, Schoppet M. Clinical implications of the osteoprotegerin/RANKL/RANK system for bone and vascular diseases. Jama. 2004; 292:490–5. [PubMed: 15280347]
7. Schoppet M, Schaefer JR, Hofbauer LC. Low serum levels of soluble RANK ligand are associated with the presence of coronary artery disease in men. Circulation. 2003; 107:e76. [PubMed: 12654623]
8. Kiechl S, Schett G, Wenning G, Redlich K, Oberhollenzer M, Mayr A, et al. Osteoprotegerin is a risk factor for progressive atherosclerosis and cardiovascular disease. Circulation. 2004; 109:2175–80. [PubMed: 15117849]
9. Viles-Gonzalez JF, Fuster V, Corti R, Valdiviezo C, Hutter R, Corda S, et al. Atherosclerosis regression and TP receptor inhibition: effect of S18886 on plaque size and composition – a magnetic resonance imaging study. Eur Heart J. 2005; 26:1557–61. [PubMed: 15734766]
10. Corti R, Osende JI, Fallon JT, Fuster V, Mizsei G, Jneid H, et al. The selective peroxisomal proliferator-activated receptor-gamma agonist has an additive effect on plaque regression in combination with simvastatin in experimental atherosclerosis: *in vivo* study by high-resolution magnetic resonance imaging. J Am Coll Cardiol. 2004; 43:464–73. [PubMed: 15013132]
11. Corti R, Osende J, Hutter R, Viles-Gonzalez JF, Zafar U, Valdivieso C, et al. Fenofibrate induces plaque regression in hypercholesterolemic atherosclerotic rabbits: *In vivo* demonstration by high-resolution MRI. Atherosclerosis. 2006
12. Zhang Z, Machac J, Helft G, Worthley SG, Tang C, Zaman AG, et al. Non-invasive imaging of atherosclerotic plaque macrophage in a rabbit model with F-18 FDG PET: a histopathological correlation. BMC Nucl Med. 2006; 6:3. [PubMed: 16725052]
13. Helft G, Worthley SG, Fuster V, Fayad ZA, Zaman AG, Corti R, et al. Progression and regression of atherosclerotic lesions: monitoring with serial noninvasive magnetic resonance imaging. Circulation. 2002; 105:993–8. [PubMed: 11864931]
14. Helft G, Worthley SG, Fuster V, Zaman AG, Schechter C, Osende JI, et al. Atherosclerotic aortic component quantification by noninvasive magnetic resonance imaging: an *in vivo* study in rabbits. J Am Coll Cardiol. 2001; 37:1149–54. [PubMed: 11263622]
15. Choi BG, Novoselsky CA, Vilahur G, Viles-Gonzalez JF, Zafar MU, Ibanez B, et al. Validation study of a semi-automated program for quantification of atherosclerotic burden. J Cardiovasc Magn Reson. 2007; 9:615–20. [PubMed: 17365244]
16. Otsu N. A threshold selection method from gray-level histograms. IEEE Trans Systems, Man, Cybernetics. 1979; 9:62–6.
17. Fujii K, Carlier SG, Mintz GS, Takebayashi H, Yasuda T, Costa RA, et al. Intravascular ultrasound study of patterns of calcium in ruptured coronary plaques. Am J Cardiol. 2005; 96:352–7. [PubMed: 16054456]
18. Fritton JC, Chinitz N, Berman D, McNamara LM, Choi BG, Badimon JJ, et al. Atherogenic treatment impairs age-related cortical bone adaptation in female rabbits. J Orthop Res. 2007 (in press). Abstract.

19. Bjarnason NH, Haarbo J, Byrjalsen I, Kauffman RF, Knadler MP, Christiansen C. Raloxifene reduces atherosclerosis: studies of optimized raloxifene doses in ovariectomized, cholesterol-fed rabbits. Clin Endocrinol (Oxf). 2000; 52:225–33. [PubMed: 10671951]

20. Vengrenyuk Y, Carlier S, Xanthos S, Cardoso L, Ganatos P, Virmani R, et al. A hypothesis for vulnerable plaque rupture due to stress-induced debonding around cellular microcalcifications in thin fibrous caps. Proc Natl Acad Sci U S A. 2006; 103:14678–83. [PubMed: 17003118]

21. LaRosa JC, Grundy SM, Waters DD, Shear C, Barter P, Fruchart JC, et al. Intensive lipid lowering with atorvastatin in patients with stable coronary disease. N Engl J Med. 2005; 352:1425–35. [PubMed: 15755765]

22. Cannon CP, Braunwald E, McCabe CH, Rader DJ, Rouleau JL, Belder R, et al. Intensive versus moderate lipid lowering with statins after acute coronary syndromes. N Engl J Med. 2004; 350:1495–504. [PubMed: 15007110]

23. Raggi P, Davidson M, Callister TQ, Welty FK, Bachmann GA, Hecht H, et al. Aggressive versus moderate lipid-lowering therapy in hypercholesterolemic postmenopausal women: Beyond Endorsed Lipid Lowering with EBT Scanning (BELLES). Circulation. 2005; 112:563–71. [PubMed: 16009795]

24. Schmermund A, Achenbach S, Budde T, Buziashvili Y, Forster A, Friedrich G, et al. Effect of intensive versus standard lipid-lowering treatment with atorvastatin on the progression of calcified coronary atherosclerosis over 12 months: a multicenter, randomized, double-blind trial. Circulation. 2006; 113:427–37. [PubMed: 16415377]

25. Choi BG, Vilahur G, Zafar MU, Cardoso L, Novoselsky CA, Yadegar D, et al. Atherosclerosis regression with selective estrogen receptor modulator therapy: an *in vivo* study of raloxifene by magnetic resonance imaging and micro-computed tomography. J Am Coll Cardiol. 2006; 47:296A. [PubMed: 16412850]

26. Collin-Osdoby P. Regulation of vascular calcification by osteoclast regulatory factors RANKL and osteoprotegerin. Circ Res. 2004; 95:1046–57. [PubMed: 15564564]

27. McClung MR, Lewiecki EM, Cohen SB, Bolognese MA, Woodson GC, Moffett AH, et al. Denosumab in postmenopausal women with low bone mineral density. N Engl J Med. 2006; 354:821–31. [PubMed: 16495394]

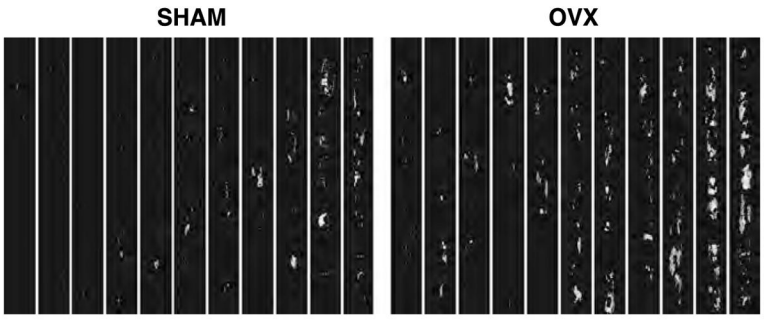

Figure 1.

Representative microcomputed tomography (μCT) images of the aorta windowed for calcification determination (each column contains a 6 centimetre segment of the infrarenal abdominal aorta) demonstrating increased vascular mineralization in the ovariectomized group. OVX: ovariectomized group; SHAM: sham-operated control group.

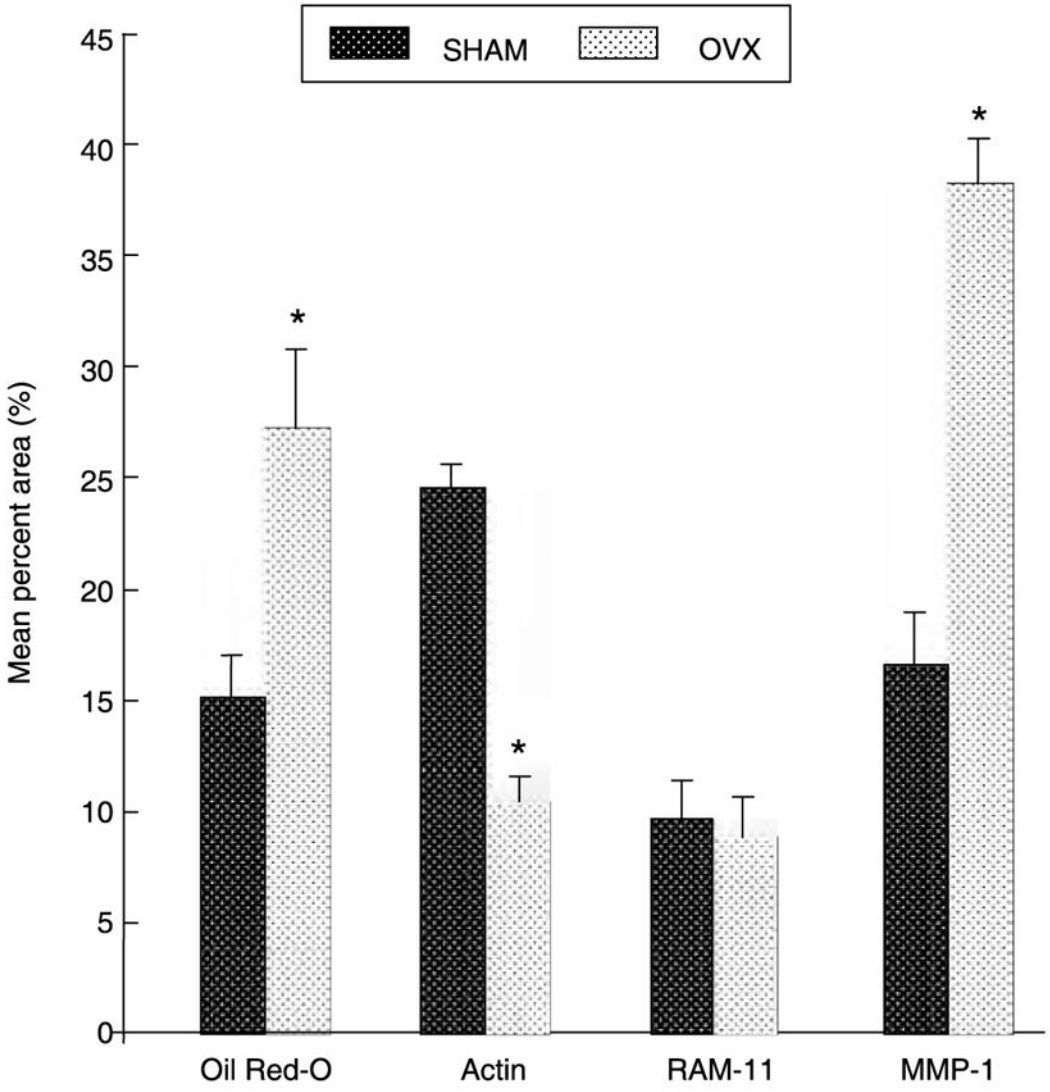

Figure 2.

Histopathological analysis of aortic vessel wall composition. Oil Red O positive area corresponds to lipid deposition, α-actin to smooth muscle, and RAM-11 to macrophage content. *$P < 0{\cdot}05$ vs. SHAM. All values expressed as mean percent area ± SEM for each treatment group. OVX: ovariectomized group ($n = 12$); SHAM: sham-operated control group ($n = 12$).

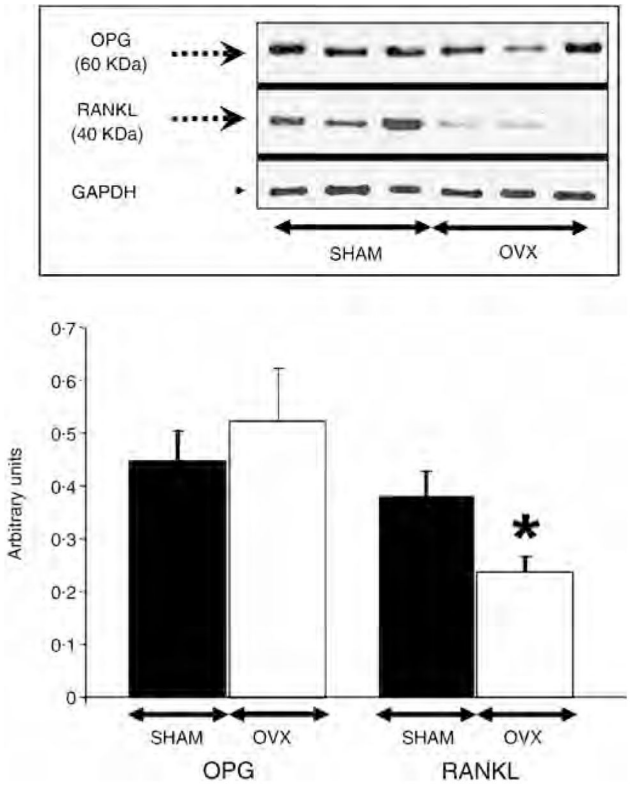

Figure 3.

Bar graph quantification and representative Western blot images for osteoprotegerin (OPG), receptor activator of nuclear factor-κB (RANKL) and GADPH (Arbitrary Units ± SEM); **P* < 0·05 vs. SHAM. There were no observable differences in GADPH level. OVX: ovariectomized group (*n* = 12); SHAM: sham-operated control group (*n* = 12).

Table 1

End of follow-up serum plasma lipid levels

	OVX	SHAM	*P*
Total cholesterol	573 ± 88	682 ± 91	0·40
LDL cholesterol	454 ± 62	605 ± 82	0·16
HDL cholesterol	55 ± 9	66 ± 11	0·47
Triglycerides	67 ± 24	59 ± 6	0·76

All serum lipid values expressed as mg dL^{-1} ± SEM, $P < 0{\cdot}05$ considered statistically significant. OVX: ovariectomized group ($n = 12$); SHAM: sham-operated control group ($n = 12$).

Table 2

Vessel wall dimensions as assessed by MRI

	Vessel wall area	Average wall thickness	Minimum wall thickness	Maximum wall thickness
OVX	4·9 ± 0·2 mm^2	586 ± 10 μm	326 ± 9 μm	858 ± 18 μm
SHAM	5·4 ± 0·1 mm^2	589 ± 11 μm	331 ± 14 μm	869 ± 15 μm

All values expressed as the mean ± SEM at end of follow-up. All *P* = n.s. OVX: ovariectomized group (*n* = 12); SHAM: sham-operated control group (*n* = 12).

Table 3

Quantitative analysis of vessel calcification by μCT and osteoprotegerin (OPG) and receptor activator of nuclear factor κB ligand (RANKL) expression by Western blot analysis

	Mineral density (mg cm^{-3})	Particle density (particles cm^{-3})	Calcific arc angle	OPG/RANKL (Arbitrary unit ratio)
OVX	8·4 ± 2·8*	94 ± 26*	33 ± 7°	1·81 ± 1·06*
SHAM	1·9 ± 0·6	33 ± 7	33 ± 5°	1·09 ± 0·81

All values expressed as mean ± SEM;

*$P < 0·05$ vs. SHAM.

OVX: ovariectomized group ($n = 12$); SHAM: sham-operated control group ($n = 12$).